PERGAMON

International Journal of Solids and Structures 37 (2000) 627–647

INTERNATIONAL JOURNAL OF SOLIDS and STRUCTURES

www.elsevier.com/locate/ijsolstr

High-accuracy plane stress and plate elements in the quadrature element method

Wei Long Chen, Alfred G. Striz*, Charles W. Bert

School of Aerospace and Mechanical Engineering, The University of Oklahoma, Room 206, 865 Asp Avenue, Norman, OK 73019-1052, USA

Received 10 June 1998; in revised form 30 December 1998

Abstract

In this paper, a high accuracy and rapid convergence hybrid approach is developed for the Quadrature Element Method (QEM) solution of two-dimensional plane stress and plate bending problems. The hybrid QEM essentially consists of a collocation method in conjunction with a Galerkin finite element technique to combine the high accuracy of the Differential Quadrature Method (DQM) with the generality of finite element formulations. This results in superior accuracy with fewer degrees of freedom than conventional FEM or FDM. The present method also extends the general application of the collocation numerical approach to fourth-order governing equation systems. Here, the influence of collocation point location is investigated. A series of numerical tests is conducted in order to assess the performance of the quadrature plane stress and plate elements in static problems. © 1999 Elsevier Science Ltd. All rights reserved.

Keywords: Quadrature element method (QEM); Differential quadrature method (DQM); Collocation method; Galerkin FEM formulation; Fourth-order equation systems; Plane stress elements; Plate elements; Numerical methods; Static structural analysis

1. Introduction

Finite element (FEM) and finite difference (FDM) methods have been employed in the past for the solution of a wide variety of problems in the field of engineering. However, both FEM and FDM typically use low-order approximating schemes, and, consequently, high accuracy is achieved only with difficulties. In recent years, in the newly emerging branch of numerical metrology, spectral and pseudospectral collocation methods have drawn special attention in the areas of fluid dynamics and heat transfer. The major advantage of this class of methods is the high accuracy attained by the resulting

* Corresponding author. Fax: +001-405-325-1088.

0020-7683/00/$ - see front matter © 1999 Elsevier Science Ltd. All rights reserved.
PII: S0020-7683(99)00028-1

discretization for much fewer nodes, or the savings in computational effort for a given accuracy. One may refer to the book by Canuto et al. (1987) for a general review.

Amongst the spectral and pseudospectral methods, the Legendre and Chebyshev pseudospectral methods are commonly used for the solution of non-perodic differential equations. However, the Legendre and Chebyshev collocation points lie unevenly spaced in the defined interval $[-1,1]$, leading to some inconvenience in application. Another numerical technique, the differential quadrature method (DQM) which was introduced by Bellman and Casti (1971) seems to possess the major advantages of the spectral method (SM) but uses even spacing. Subsequently, the DQM will provide for an easier transformation between the physical and the computational domains. More detailed discussions and review articles have appeared in recent years, e.g., Quan and Chang (1989), Bernardi and Maday (1991).

Difficulties in applying the collocation method to practical engineering problems arise whenever the geometry to be considered departs from a simple rectangle and when high resolution boundary conditions are needed. Here, the limitations caused by using global basis functions become an unfavorable feature. Also, if there are discontinuities in the computational domain, then globally continuous interpolation functions are not suitable for an approximation of the physical model. As an improvement, many domain decomposition techniques have been proposed. Amongst these methods, Patera (1984) used a variational formulation which combines the generality of the FEM and the accuracy of the spectral method (SM). He named this the spectral element method (SEM) which is one of the commonly used methods.

The differential quadrature method (DQM) has been applied to the analysis of various single structural components such as bars, beams, membranes, and plates by Striz et al. (1988), Bert et al. (1989), and Wang et al. (1993). In some cases, the SM and the DQM or the SEM and QEM are identical. For instance, when applying these two classes of methods to second-order governing equations, the only major difference would be the grid spacing. However, most of the problems encountered in the field of solid mechanics are high-order systems with more than one kind of boundary condition at each edge. To apply boundary conditions in fourth-order systems, a boundary approximation approach was developed by Jang et al. (1989), the δ-type grid arrangement. This kind of approximation is quite efficient for clamped boundaries, that is, if both the Dirichlet and Neumann boundary conditions are zero. For other kinds of boundary conditions, however, one will find that the required increased programming efforts inflict losses on the simplicity and efficiency of the DQ scheme when compared with the second-order systems. Most of all, the accuracy of the approximating solution is difficult to determine. The reason is that, for arbitrarily distributed grid points, quadrature is usually obtained by inverting an ill-conditioned Vandermonde matrix where the numerical inversion procedure becomes unstable for large numbers of grid points due to limited digits used in computers. Consequently, the accuracy of the solution deteriorates as the number of grid points increases. Also, another disadvantage to the δ-type grid arrangement is that it is not suitable for the development of domain decomposition techniques. Even if the node number in a subdomain is not too large, when one assembles the stiffness matrix, one will find that the orders of the weighting coefficients for interelement nodal points and for interior nodal points are quite different. Thus, in the procedures for inverting such stiffness matrices, truncation errors will cause inaccuracies. This means that an increase in nodal points will not necessarily guarantee a good solution for multi-domain problems. With the improvements to the high-order DQM shown by Chen et al. (1997), and applied by Striz et al. (1997) to the free vibration of plates, domain decomposition techniques become easier for fourth-order systems. Deciding the DQ weighting coefficients for such a system analytically could be cumbersome compared with second-order systems, although it seems possible. For convenience, it is advantageous to calculate the weighting coefficients for fourth-order systems numerically. One will then find that the improved scheme tends to converge for a mesh of up to 15×15 nodes for a two dimensional system which could not exceed 11×11 nodes in the previous scheme. Of course, if the number of nodal points for a single domain is

large, such as 30×30, analytical calculation of the weighting coefficients is necessary in order to minimize numerical errors caused by inverting ill-conditioned matrices. This is beyond the scope of the present study. For moderately large node numbers (less than 15×15), numerically deciding the weighting coefficients seems reasonable. Finally, the stiffness matrices need to be inverted numerically when solving for the field variables.

In the following plane stress problem, we will present a numerical technique which is an extension of the spectral element method. Finally, for plate bending problems, a numerical technique combining a variational formulation and a fourth-order collocation approach to the solution of fourth-order governing equations will be introduced.

2. Comparisons of QEM with other high accuracy schemes

2.1. Formulation for single boundary condition at domain ends

To illustrate the hybrid method used in the QEM and to compare it with other approximate high-order numerical methods mentioned in the previous section, we shall investigate the convergence of a simple one-dimensional ODE with known exact solution which will be convenient for direct comparison. Consider the solution of

$$\frac{\mathrm{d}^2\phi}{\mathrm{d}x^2} + \phi + x = 0,\ 0 \le x \le 1,\ \phi(0) = \phi(1) = 0. \tag{1}$$

The functional I corresponding to Eq. (1) is given by

$$I = \frac{1}{2}\int_0^1 \left[-\left(\frac{\mathrm{d}\phi}{\mathrm{d}x}\right)^2 + \phi^2 + 2\phi x \right] \mathrm{d}x. \tag{2}$$

For the spatial discretization by the QEM, the global coordinate x defined in the interval $[a,b]$ can be transformed to the local coordinate system $\bar{x}$, which is defined on the interval $[-1,1]$, such that:

$$\bar{x} = \frac{2}{(b-a)}(x-a) - 1. \tag{3}$$

Let the e-th element be defined in the interval $[a,b]$ in the global coordinate system. The series expansion for the function $\phi(\bar{x})$ in the e-th element can be written as

$$\phi(\bar{x}) \approx \phi_n^e(\bar{x}) = \sum_{k=0}^{n} N_k(\bar{x})\phi_k^e = \lfloor N \rfloor \{\phi^e\}. \tag{4}$$

Here, $N_k(\bar{x})$ are the basis functions which are locally continuous over the e-th elemental domain $[a,b]$, and ϕ_k^e are the coefficients. The superscript e denotes the e-th element. The interpolating basis functions $N_k(\bar{x})$ can be calculated as follows:

$$\lfloor N \rfloor = \lfloor \bar{x} \rfloor \lfloor v_0 \rfloor^{-T}, \tag{5}$$

where

$$\lfloor \bar{x} \rfloor = \lfloor 1\ \bar{x}\ \ldots\ \bar{x}^n \rfloor \tag{6}$$

and $[v_0]$ is the Vandermonde matrix,

$$[v_0] = \begin{bmatrix} 1 & 1 & \dots & 1 \\ \bar{x}_0 & \bar{x}_1 & \dots & \bar{x}_n \\ \vdots & \vdots & \vdots & \vdots \\ \bar{x}_0^n & \bar{x}_1^n & \dots & \bar{x}_n^n \end{bmatrix}. \tag{7}$$

Using the necessary conditions to make I stationary,

$$\frac{\partial I}{\partial \phi_i} = \sum_{e=1}^{E} \frac{\partial I^e}{\partial \phi_i} = 0, \tag{8}$$

one can construct the equation

$$\sum_{e=1}^{E} [K^e]\{\phi^e\} = \sum_{e=1}^{E} \{P^e\}, \tag{9}$$

where

$$[K^e] = \int_a^b \left\{ -\left[\frac{\mathrm{d}N}{\mathrm{d}x}\right]^T \left[\frac{\mathrm{d}N}{\mathrm{d}x}\right] + \lfloor N \rfloor^T \lfloor N \rfloor \right\} \mathrm{d}x = \left\{ \frac{-2}{(b-a)} [v_0]^{-1} [r] [v_0]^{-T} + \frac{(b-a)}{2} [v_0]^{-1} [s] [v_0]^{-T} \right\}; \tag{10}$$

$$[r] = (r)_{(n+1)\times(n+1)},\ [s] = (s)_{(n+1)\times(n+1)}, \tag{10a}$$

$$r_{lm} = \int_{-1}^{1} \frac{\mathrm{d}\bar{x}^l}{\mathrm{d}\bar{x}} \frac{\mathrm{d}\bar{x}^m}{\mathrm{d}\bar{x}} \, \mathrm{d}\bar{x} = \begin{cases} \dfrac{2lm}{l+m-1} & l+m \quad \text{even} \\ 0 & l+m \quad \text{odd} \end{cases} \tag{10b}$$

and

$$s_{lm} = \int_{-1}^{1} \bar{x}^l \bar{x}^m \, \mathrm{d}x = \begin{cases} \dfrac{2}{l+m+1} & l+m \quad \text{even} \\ 0 & l+m \quad \text{odd} \end{cases}. \tag{10c}$$

Also, the characteristic vector for the e-th element can be considered as

$$\{p^e\} = -\int_a^b [v_0]^{-1} \{\bar{x}\} x \, \mathrm{d}x. \tag{11}$$

Assembling Eqs. (9)–(11), one obtains

$$\sum_{e=1}^{E} [K^e]\{\phi\} = \sum_{e=1}^{E} \{P^e\}. \tag{12}$$

In a QEM approach, the $(n + 1)$ interpolating points in the local coordinate system would be uniform such that

$$\bar{x}_i = \frac{2i-n}{n};\ i = 0, \dots, n. \tag{13}$$

In a SEM approach, the $(n+1)$ interpolating points in the local coordinate system would be

$$\bar{x}_i = -\cos\frac{\pi i}{n}\ i = 0,1,2,\ldots,n \text{ for a (Gauss} - \text{Lobatto) Chebyshev grid,}$$

or

$$\bar{x}_0 = -1, \bar{x}_n = 1, \text{ and the } (N-1) \text{ roots of } \frac{\mathrm{d}P_n}{\mathrm{d}\bar{x}} = 0 \text{ for a Legendre grid,} \tag{14}$$

where, P_n denotes the n-th order Legendre polynomials. For the cases of uniform, Chebyshev, or Legendre collocation points, closed-form expressions for the basis functions exist. Although the algebraic system, derived in discretized form in Eq. (5), requires the calculation of the inverse of a full Vandermonde matrix, as long as the order of the polynomial is not too large the adverse influence is not significant. The advantage in expressing the basis functions in the form of Eq. (5) is that the formulation can be adjusted for simplicity and any general situation can be considered. This will greatly reduce difficulties encountered when writing the numerical discretization in a general context for various grid spacings in multi-dimensional and fourth- or even higher-order governing equations. Also, once the Vandermonde matrix in Eq. (7) is determined, efficiency and formulation efforts for different grid spacings will be the same when calculating the stiffness matrix.

On the other hand, the derivative of the series $\phi_n^e(\bar{x})$ in Eq. (4) serves as an approximation of $\phi'(\bar{x})$. Since the ϕ_n^e are not explicit functions of the variable x, the derivative of $\phi_n^e(\bar{x})$ simply involves the derivatives of the basis functions. The derivative of a function at a specific collocation point $\bar{x}_i$ is evaluated by applying the formula

$$\phi_n'^e(\bar{x}_i) = \frac{\mathrm{d}}{\mathrm{d}\bar{x}}\lfloor N\rfloor\{\phi^e\} = \lfloor 0\ 1\ 2\bar{x}_i\ \ldots\ n\bar{x}_i^{n-1}\rfloor[v_0]^{-T}\{\phi^e\}. \tag{15}$$

If the derivatives of all collocation points are calculated using Eq. (15), one obtains the weighting coefficients of the first derivative in matrix form $[A_x]$.

$$\frac{\mathrm{d}}{\mathrm{d}\bar{x}}\phi_n^e(\bar{x}) = \begin{bmatrix} 0 & 1 & 2\bar{x}_0 & \ldots & n\bar{x}_0^{n-1} \\ 0 & 1 & 2\bar{x}_i & \ldots & n\bar{x}_1^{n-1} \\ \vdots & \vdots & \vdots & \ldots & \vdots \\ 0 & 1 & 2\bar{x}_{n-1} & \ldots & n\bar{x}_{n-1}^{n-1} \\ 0 & 1 & 2\bar{x}_n & \ldots & n\bar{x}_n^{n-1} \end{bmatrix}[v_0]^{-T}\{\phi^e\} = [A_x]\{\phi^e\}. \tag{16}$$

The weighting coefficients for the second and n-th order derivatives can then be computed as

$$\frac{\mathrm{d}^2}{\mathrm{d}\bar{x}^2} = \left(\frac{\mathrm{d}}{\mathrm{d}\bar{x}}\right)\left(\frac{\mathrm{d}}{\mathrm{d}\bar{x}}\right) = [A_x][A_x]$$

and

$$\frac{\mathrm{d}^n}{\mathrm{d}\bar{x}^n} = \left(\frac{\mathrm{d}}{\mathrm{d}\bar{x}}\right)\left(\frac{\mathrm{d}^{n-1}}{\mathrm{d}\bar{x}^{n-1}}\right) = \underbrace{[A_x][A_x]\ldots[A_x]}_{n}. \tag{17}$$

Since the steps of the above process are all linear operations, in practice, the linear operators are combined factor-by-factor to a single matrix operator which, when multiplied into the vector of values of the functions at the collocation points, yields the vector of derivatives, with specific physical meaning

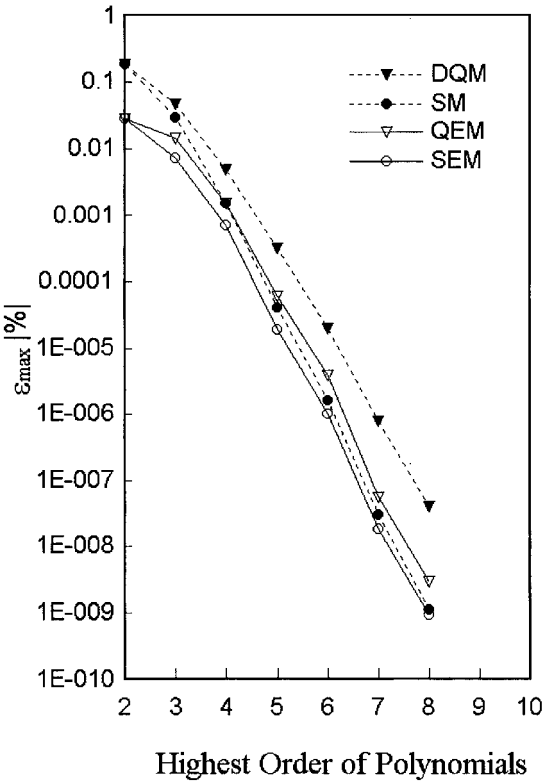

Fig. 1. Comparison of several high-order numerical schemes for one-dimensional ODE.

and importance, at these points. This expression is especially useful when computing the derivatives of a field variable at the collocation points, such as in stress recovery, which involves the derivatives of the displacements. The SEM and SM results in the present example are obtained using Chebyshev basis functions, although Legendre series have been applied to a number of problems, and would perform equally well in the present context. For details on other high accuracy numerical schemes such as DQM, SM, and SEM, one can refer to Bellman and Casti (1971), Canuto et al. (1987), Quan and Chang (1989) and Patera (1984). The numerical results for the QEM compared with DQM, SM, and SEM results are plotted in Fig. 1. As expected, all these methods converge exponentially with respect to an increase in the number of discretized points, at a rate much faster than conventional FDM and FEM, which are relatively insensitive to the number of nodes. In Fig. 1,

$$\varepsilon_{\max} = \|\phi_{\text{numerical}} - \phi_{\text{exact}}\| \tag{18}$$

denotes the maximum absolute error at any discretized point in the computational domain.

2.2. Extension of formulation to two boundary conditions at each domain end

Similar to the one-dimensional approach described in the previous section, an extension of the method to fourth-order governing equation systems is developed. As mentioned previously, the difficulty in the formulation arises from the two boundary conditions at each domain end. With the given

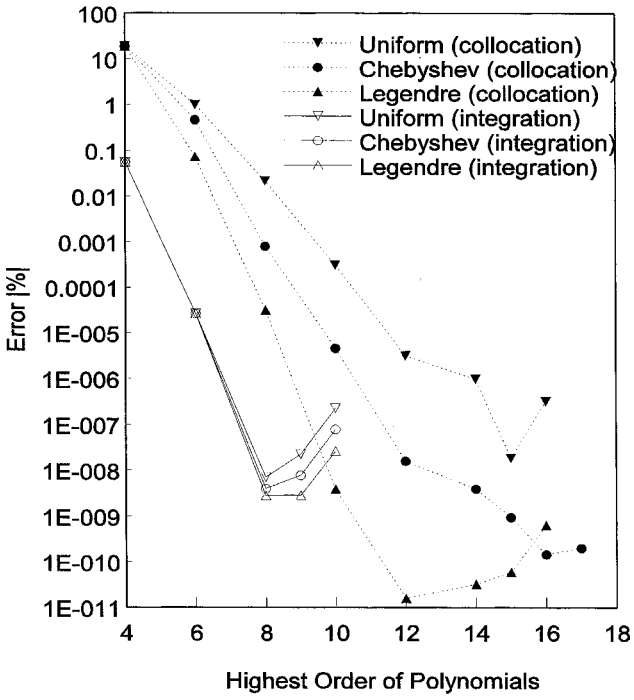

Fig. 2. Convergence comparison of the critical load for a uniform pinned–pinned column by various methods.

extensions, two or even more boundary conditions and different collocation points can be handled without difficulties. Details of this extension can be found in Chen et al. (1997).

A brief description is given in the following. A one-dimensional fourth-order governing equation with field variable $w(\bar{x})$ is considered. The interpolating basis functions $N_k(\bar{x})$ are calculated similar to Eq. (4). Extra conditions at the end points are added to meet the two boundary conditions at each end, such that the corresponding basis functions for all $(n+1)$ collocation points are

$$\lfloor N \rfloor = \lfloor 1 \ \bar{x} \ \bar{x}^2 \ \ldots \ \bar{x}^{n+2} \rfloor [c_0]^{-1} \text{ for } \bar{x}_i = \bar{x}_1, \bar{x}_2, \ldots, \bar{x}_{n-1} \tag{19}$$

and

$$\lfloor N \rfloor = \left(\lfloor 1 \ \bar{x} \ \bar{x}^2 \ \ldots \ \bar{x}^{n+2} \rfloor + \lfloor 0 \ 1 \ 2\bar{x} \ \ldots \ (n+2)\bar{x}^{n+1} \rfloor \right) [c_0]^{-1} \text{ for } \bar{x}_i = \bar{x}_0, \bar{x}_n, \tag{20}$$

where

$$[c_0] = \begin{bmatrix} 1 & \bar{x}_0 & \bar{x}_0^2 & \ldots & \bar{x}_0^{n+1} & \bar{x}_0^{n+2} \\ 0 & 1 & 2\bar{x}_0 & \ldots & (n+1)\bar{x}_0^{n} & (n+2)\bar{x}_0^{n+1} \\ 1 & \bar{x}_1 & \bar{x}_1^2 & \ldots & \bar{x}_1^{n+1} & \bar{x}_1^{n+2} \\ \vdots & \vdots & \vdots & \vdots & \vdots & \vdots \\ 1 & \bar{x}_1 & \bar{x}_n^2 & \ldots & \bar{x}_n^{n+1} & \bar{x}_n^{n+2} \\ 0 & 1 & 2\bar{x}_n & \ldots & (n+1)\bar{x}_n^{n} & (n+2)\bar{x}_n^{n+1} \end{bmatrix}. \tag{21}$$

From Eqs. (19) and (20), the variable w can be assumed as

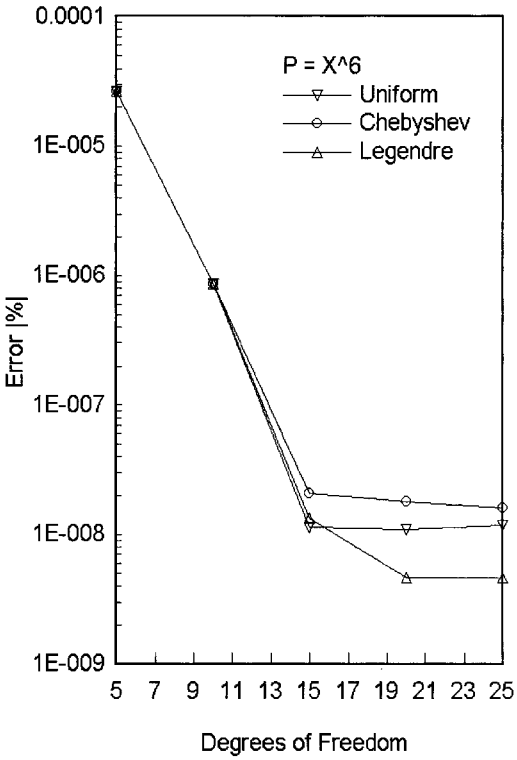

Fig. 3. Convergence of QEM approach for critical load of uniform pinned–pinned column (fixed polynomial order = 6).

$$w(\bar{x}) = \sum_{i=1}^{n-1}[N_{i1}w_i] + \sum_{i=0,n}\left[N_{i1}w_i + N_{i2}\left(\frac{\mathrm{d}w}{\mathrm{d}\bar{x}}\right)_i\right]. \tag{22}$$

Using Eq. (22), one observes that the first derivatives of the field variable w at the end points are constrained. Also, similar to Eq. (16), the weighting coefficient matrix for the first derivative, which may be applied in calculating the derivatives of the field variables, is found to be:

$$[A_x] = \begin{bmatrix} 0 & 1 & 2\bar{x}_0 & \dots & (n+1)\bar{x}_0^n & (n+2)\bar{x}_0^{n+1} \\ 0 & 0 & 2 & \dots & (n+1)n\bar{x}_0^{n-1} & (n+2)(n+1)\bar{x}_0^n \\ 0 & 1 & 2\bar{x}_i & \dots & (n+1)\bar{x}_0^n & (n+2)\bar{x}_1^{n+1} \\ \vdots & \vdots & \vdots & \vdots & \vdots & \vdots \\ 0 & 1 & 2\bar{x}_n & \dots & (n+1)\bar{x}_n^n & (n+2)\bar{x}_n^{n+1} \\ 0 & 0 & 2 & \dots & (n+1)n\bar{x}_n^{n-1} & (n+2)(n+1)\bar{x}_n^n \end{bmatrix} [c_0]^{-1}. \tag{23}$$

To illustrate the fourth-order collocation method, here, the numerical convergence of the buckling of a Bernoulli–Euler beam with pinned–pinned boundary conditions was investigated. The governing equation can be expressed as

$$EI\frac{\mathrm{d}^4 w}{\mathrm{d}x^4} = q(x) - N\frac{\mathrm{d}^2 w}{\mathrm{d}x^2}, \tag{24}$$

where w is the transverse displacement function in the y-direction, E and I denote the modulus of elasticity and the principal moment of inertia about the z-axis, and N is the axial load, respectively. Applying the stated numerical techniques to this column buckling problem, convergence studies for different grid spacings are presented in Fig. 2, together with the integration approach of the QEM.

In the solution of the buckling load, one observes that approximations of excessively high order will eventually result in an overdetermined solution and cause a numerical instability. Although this kind of instability is problem dependent, it is inevitable for this class of methods if no special treatment is applied to the overdetermined solution. However, if an element-type integration approach as in the QEM is used, the order of the approximation polynomials is fixed in each element. Therefore, one may find it more numerically stable with an increase in the number of nodes. Fig. 3 shows the different grid spacings have little influence on the convergence of the hybrid QEM scheme in fourth-order systems. In real applications, element type domain decomposition techniques will provide a more flexible scheme which can be used to isolate discontinuies in the computational domain or on the boundaries and provide fast convergence.

Generally speaking, the previously mentioned methods can be classified into two categories, pure collocation approaches, such as the DQM and SM; and hybrid approaches using collocation and integration, such as the SEM and QEM. It is well known that the choice of the collocation points and orthogonality are crucial to the accuracy of the pure collocation approach; therefore, one can see that the SM is more accurate than the DQM for the given problems. However, when hybrid approaches are developed, one finds that their accuracy is quite insensitive to the grid spacing as opposed to the pure collocation approaches. That is, the order of the chosen polynomial functions is more crucial to the rapidity of convergence for the range of polynomial orders discussed in this study. In the following section, both SEM and QEM will be implemented in solving the plane stress problem. Their accuracy will be demonstrated and comparisons of both methods will be presented.

3. Static analysis by rectangular plane stress quadrature element

Here, the plane stress elements are assumed to be rectangular as shown in Fig. 4(a–c). The nodal points are located at the collocation points, which will be discussed in more detail later. Each nodal point in the element possesses two degrees of freedom, u and v, which denote the displacements in the x- and y-directions, respectively.

The two-dimensional trial functions for the displacements, u and v, can be assumed as

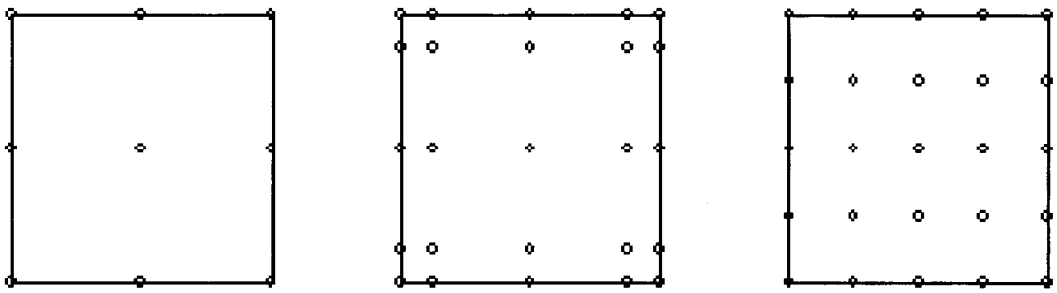

Fig. 4. (a) 18 D.o.F. Lagrange biquadratic plane stress element, (b) 50 D.o.F. spectral plane stress element, (c) 50 D.o.F. quadrature plane stress element.

$$u(\bar{x},\bar{y}) = \sum_{j=0}^{N_x}\sum_{k=0}^{N_y} N_j(\bar{x})N_k(\bar{y})u_{jk}, \quad v(\bar{x},\bar{y}) = \sum_{j=0}^{N_x}\sum_{k=0}^{N_y} N_j(\bar{x})N_k(\bar{y})v_{jk}. \tag{25}$$

The superbar indicates the local element coordinate system given by

$$\bar{x} = \frac{2}{(x_2 - x_1)}(x - x_1) - 1, \quad \bar{y} = \frac{2}{(y_2 - y_1)}(y - y_1) - 1 \tag{26}$$

and N_j and N_k are the interpolation polynomials in the x- and y-directions, respectively. The derivations of N_j and N_k for either Lagrange or Chebyshev polynomials are extensions from the previous one-dimensional case.

3.1. Formulation of quadrature plane stress element

For a plane stress state, the equilibrium equations in terms of the stresses can be expressed as

$$\frac{\partial \sigma_{xx}}{\partial x} + \frac{\partial \tau_{xy}}{\partial y} + b_x = 0, \quad \frac{\partial \tau_{xy}}{\partial x} + \frac{\partial \sigma_{yy}}{\partial y} + b_y = 0, \tag{27}$$

where b_x and b_y denote body forces in the x- and y-directions, respectively.

For small deformations, the strain–displacement relations can be written in the following form:

$$\varepsilon_x = \frac{\partial u}{\partial x}, \quad \varepsilon_y = \frac{\partial v}{\partial y}, \quad \gamma_{xy} = \frac{\partial u}{\partial y} + \frac{\partial v}{\partial x}. \tag{28}$$

Substituting the trial functions from Eq. (25) into Eq. (28), the strain–displacement equations can be rewritten as

$$\begin{Bmatrix} \varepsilon_x \\ \varepsilon_y \\ \gamma_{xy} \end{Bmatrix} = \begin{bmatrix} \frac{\partial f_{00}}{\partial x} & 0 & \frac{\partial f_{01}}{\partial x} & 0 & \cdots & \frac{\partial f_{jk}}{\partial x} & 0 \\ 0 & \frac{\partial f_{00}}{\partial y} & 0 & \frac{\partial f_{01}}{\partial y} & \cdots & 0 & \frac{\partial f_{jk}}{\partial y} \\ \frac{\partial f_{00}}{\partial y} & \frac{\partial f_{00}}{\partial x} & \frac{\partial f_{01}}{\partial y} & \frac{\partial f_{01}}{\partial x} & \cdots & \frac{\partial f_{jk}}{\partial y} & \frac{\partial f_{jk}}{\partial x} \end{bmatrix} \begin{Bmatrix} u_{00} \\ v_{00} \\ \vdots \\ \vdots \\ u_{jk} \\ v_{jk} \end{Bmatrix} = [A]\{q\}. \tag{29}$$

Here, $[A]$ is a compound derivative operator in matrix form, and the f_{jk} are trial functions

$$f_{jk} = N_j(\bar{x})N_k(\bar{y}). \tag{30}$$

Also, the stress–strain relations are of the form

$$\begin{Bmatrix} \sigma_x \\ \sigma_y \\ \tau_{xy} \end{Bmatrix} = \begin{bmatrix} c_{11} & c_{12} & c_{13} \\ c_{12} & c_{22} & c_{23} \\ c_{13} & c_{23} & c_{33} \end{bmatrix} \begin{Bmatrix} \varepsilon_x \\ \varepsilon_y \\ \gamma_{xy} \end{Bmatrix} \tag{31}$$

or, abbreviated,

$$\{\sigma\} = [c]\{\varepsilon\} = [c][A]\{q\}. \tag{32}$$

To derive the element stiffness matrix and equations, one can use the principle of minimum potential

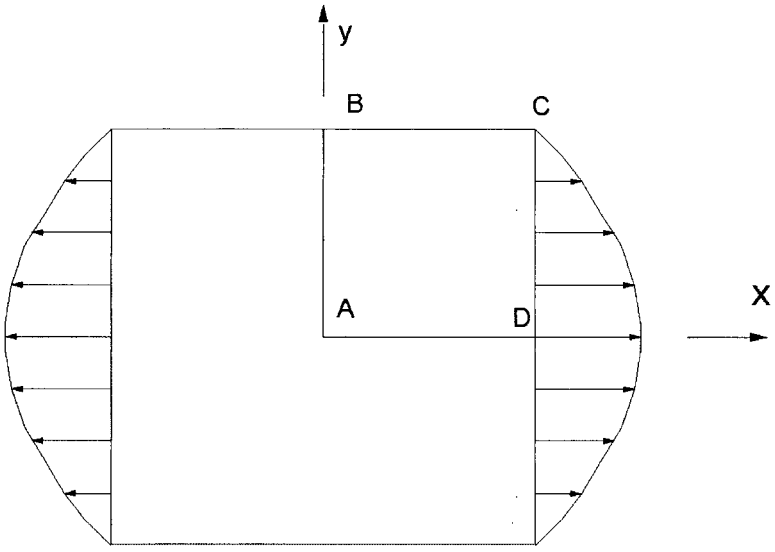

Fig. 5. Plate under plane parabolic load.

energy. The strain energy is given by

$$U = \frac{1}{2}\int\int\int_V \{\varepsilon\}^T\{\sigma\}\mathrm{d}V = \frac{1}{2}\int\int\int_V \{\varepsilon\}^T[c]\{\varepsilon\}\mathrm{d}V, \tag{33}$$

where V is the volume.

Applying Castigliano's first theorem gives

$$F_i = \frac{\partial U}{\partial q_i}. \tag{34}$$

Differentiating the strain energy by performing differential quadrature procedures similar to those used in the one-dimensional case with respect to each degree of freedom of the element, one can construct the final matrix as

$$[K]\{q\} = \{F\}, \tag{35}$$

where the stiffness matrix is

$$[K] = \int\int\int_V [A]^T[c][A]\mathrm{d}V \tag{36}$$

and $\{F\}$ is the vector of external loads.

3.2. Numerical application

The plane stress problem illustrated in Fig. 5 is used to test the plane stress element. It models an isotropic square plate with uniform thickness under a parabolically distributed stress on two opposite sides with the other two sides traction free. The distributed stress σ_x acting on the boundaries is

Table 1
Numerical displacement results for parabolically loaded plane stress problem[a]

	$v_B \frac{10Et}{(1-\nu^2)\sigma_0 L}$	$u_C \frac{10Et}{(1-\nu^2)\sigma_0 L}$	$v_C \frac{100Et}{(1-\nu^2)\sigma_0 L}$	$u_D \frac{10Et}{(1-\nu^2)\sigma_0 L}$
A	−1.522267	1.29132	1.8698	5.072967
(16,144)[c]	(1.5×10^{-3})[d]	(1.1×10^{-2})	(4.8×10^{-2})	(1.0×10^{-4})
B	−1.520537	1.27841	1.7951	5.072867
(1,40)	(4.0×10^{-4})	(8.9×10^{-4})	(6.2×10^{-3})	(1.2×10^{-4})
C	−1.520537	1.27841	1.7951	5.072867
(1,40)	(4.0×10^{-4})	(8.9×10^{-4})	(6.2×10^{-3})	(1.2×10^{-4})
D	−1.519920	1.27727	1.7836	5.073486
(4,144)	(5.3×10^{-6})	(2.3×10^{-6})	(1.5×10^{-6})	(1.6×10^{-6})
E	−1.519920	1.27727	1.7836	5.073486
(4,144)	(5.3×10^{-6})	(2.3×10^{-6})	(1.5×10^{-6})	(1.6×10^{-6})
F	−1.519824	1.27922	1.7590	5.073691
(4,144)	(6.8×10^{-5})	(1.5×10^{-3})	(1.4×10^{-2})	(1.7×10^{-6})
G	−1.519795	1.28009	1.7499	5.073368
(4,144)	(8.7×10^{-5})	(2.2×10^{-3})	(1.9×10^{-2})	(2.1×10^{-6})
Exact[b]	−1.519928	1.27727	1.7837	5.073478

[a] A: Sixteen Lagrange basis square quadrature elements [Fig. 4(a)], highest order of interpolation function is 4. B: One Chebyshev basis square spectral element [Fig. 4(b)], highest order of interpolation function is 8. C: One Lagrange basis square quadrature element [Fig. 4(c)], highest order of interpolation function is 8. D: Four Chebyshev basis square spectral elements [Fig. 4(b)], highest order of interpolation function is 8. E: Four Lagrange basis square quadrature elements [Fig. 4(c)], highest order of interpolation function is 8. F: Four Lagrange basis quadrature elements [Fig. 4(c)], highest order of interpolation function is 8, $b/a = 3$ (Fig. 6). G: Four Lagrange basis quadrature elements [Fig. 4(c)], highest order of interpolation function is 8, $b/a = 7$ (Fig. 6).

[b] Cowper et al. (1970).

[c] (m, n), m = number of elements, n = degrees of freedom.

[d] Absolute value of relative difference, defined as: |(computational−exact)|/|exact|.

$$\sigma_x = \sigma_0\left[1 - 4\frac{x^2}{L^2}\right]. \tag{37}$$

The length, thickness, Young's modulus, and Poisson's ratio of the square plate are L, t, E and ν, respectively.

The problem is solved using the plane stress elements shown in Fig. 4(a–c) and various grids for the quarter plate. Some selected numerical results for displacements and stresses at the points A, B, C, and D shown in Fig. 5 are presented in Tables 1 and 2.

3.3. Result and discussion

An 'exact' solution was obtained by using enough terms of a trigonometric and hyperbolic series expansion (see Cowper et al. (1970)) to compare with the QEM numerical results. The displacements and stresses at the corner points A, B, C, D are presented in Tables 1 and 2, respectively. From these tables, one can observe that the higher order approximations result in high accuracy which is difficult to achieve by conventional low-order approximation, or alternatively, that they obtain good accuracy with coarse mesh models. However, very-high-order approximation does not mean infinite convergence, since it not only causes numerical problems but also becomes overdetermined for simpler solution forms. Considering flexibility and efficiency for further developments, a 25 nodal point element seems to represent an optimum. Also, different from the one-dimensional problem, both QEM and SEM show the same accuracy of the numerical results in this two-dimensional problem. Therefore, when a

Table 2
Numerical results for parabolically loaded plane stress problem[a]

	$10\sigma_{xA}/\sigma_0$	$10\sigma_{yA}/\sigma_0$	$10\sigma_{xB}/\sigma_0$	$10\sigma_{yB}/\sigma_0$	$10\sigma_{xC}/\sigma_0$	$10\sigma_{yC}/\sigma_0$
A	8.55498	−1.46901	4.19128	0.07903	−0.178	−0.210
(16,144)[c]	(4.1×10^{-3})[d]	(4.2×10^{-2})	(2.1×10^{-2})	(—)	(—)	(—)
B	8.64238	−1.35761	3.99255	0.00553	−0.2422	−0.2422
(1,40)	(6.0×10^{-3})	(3.7×10^{-2})	(1.1×10^{-1})	(—)	(—)	(—)
C	8.64238	−1.35761	3.99255	0.00553	−0.2422	−0.2422
(1,40)	(6.0×10^{-3})	(3.7×10^{-2})	(1.1×10^{-1})	(—)	(—)	(—)
D	8.59319	−1.40681	4.10593	0.00311	−0.0470	−0.0470
(4,144)	(3.2×10^{-4})	(1.9×10^{-3})	(1.9×10^{-4})	(—)	(—)	(—)
E	8.59319	−1.40681	4.10593	0.00311	−0.0470	−0.0470
(4,144)	(3.2×10^{-4})	(1.9×10^{-3})	(1.9×10^{-4})	(—)	(—)	(—)
F	8.59319	−1.40568	4.09233	0.0143	−0.0343	−0.1713
(4,144)	(1.5×10^{-3})	(2.7×10^{-3})	(3.5×10^{-4})	(—)	(—)	(—)
G	8.61504	−1.40187	4.06266	0.0207	−0.0102	−0.2304
(4,144)	(2.9×10^{-3})	(5.4×10^{-3})	(1.1×10^{-2})	(—)	(—)	(—)
Exact[b]	8.59046	−1.40954	4.10670	0	0	0

[a] A: Sixteen Lagrange basis square quadrature elements [Fig. 4(a)], highest order of interpolation function is 4. B: One Chebyshev basis square spectral element [Fig. 4(b)], highest order of interpolation function is 8. C: One Lagrange basis square quadrature element [Fig. 4(c)], highest order of interpolation function is 8. D: Four Chebyshev basis square spectral elements [Fig. 4(b)], highest order of interpolation function is 8. E: Four Lagrange basis square quadrature elements [Fig. 4(c)], highest order of interpolation function is 8. F: Four Lagrange basis quadrature elements [Fig. 4(c)], highest order of interpolation function is 8, $b/a = 3$ (Fig. 6). G: Four Lagrange basis quadrature elements [Fig. 4(c)], highest order of interpolation function is 8, $b/a = 7$ (Fig. 6).
[b] Cowper et al. (1970).
[c] (m, n), m = number of elements, n = degrees of freedom.
[d] Absolute value of relative difference, defined as: |(computational−exact)|/|exact|.

transformation between the computational domain and the physical domain is needed, a moderately-high-order element QEM will provide the more flexible scheme, that is, a large number of nodal points, to attain higher accuracy. In the quadrature element method, the basis functions are more complete; therefore, it achieves C^0 and C^1 accuracy, that is, both displacements and stresses are more accurate than for the same degree-of-freedom FEM models.

When different aspect ratio elements are implemented in the problem (see Fig. 6) the maximum and minimum principal stresses are shown in Fig. 7(a,b), respectively. Here, detailed stress distributions for two models, one with four elements of aspect ratio 1 and one with four elements of aspect ratios 1, 7, 1 and 1/7 are computed from Eq. (31) by calculating the compound differential operator and the field variables, u and v, depending on the collocation points used. It is encouraging to see that aspect ratio has much less influence on the accuracy of the present method than on low-order numerical schemes, even if the stretching of an element is severe.

4. Static analysis by rectangular quadrature plate element

4.1. Formulation of quadrature plate element

The quadrature plate element is formulated based on the discrete Kirchhoff assumptions. Then, the governing equation for an isotropic thin plate undergoing small deflections is given by

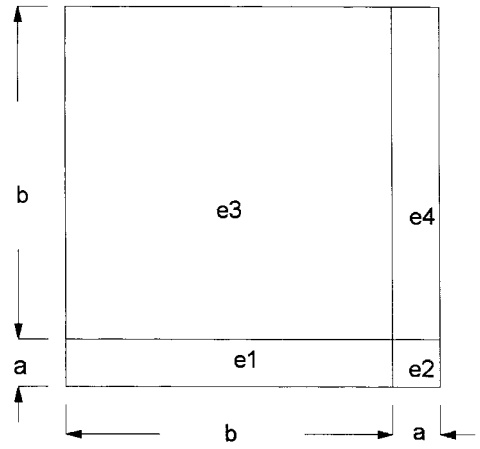

Fig. 6. Element arrangement for plane stress problem.

$$\frac{\partial^4 w}{\partial x^4} + 2\frac{\partial^4 w}{\partial x^2 \partial^2 y} + \frac{\partial^4 w}{\partial y^4} = \frac{q(x,y)}{D}, \tag{38}$$

where $q(x,y)$ represents the distributed transverse load and D is the plate rigidity, such that $D = Eh^3/12(1-\nu^2)$. The quadrature plate element is closely related to the serendipity Lagrange element, but uses basis functions of higher order. Interelement compatibilities C^0 and C^1 are met exactly at the midsurface. A twenty-five-node rectangular element with 49 degrees of freedom is shown in Fig. 8 and described in Table 3. The displacement field of the 49 D.o.F. quadrature plate element is expressed in terms of polynomial type basis functions such that the displacement of the element can be assumed as:

$$\begin{aligned} w(\bar{x},\bar{y}) = &\sum_{i=1,5,9,13}\left[N_{i1}w_i + N_{i2}\left(\frac{\partial w}{\partial \bar{x}}\right)_i + N_{i3}\left(\frac{\partial w}{\partial \bar{y}}\right)_i + N_{i4}\left(\frac{\partial^2 w}{\partial \bar{x}\partial \bar{y}}\right)_i\right] + \sum_{i=2,3,4,10,11,12}\left[N_{i1}w_i + \right. \\ &\left. N_{i2}\left(\frac{\partial w}{\partial \bar{y}}\right)_i\right] + \sum_{i=6,7,8,14,15,16}\left[N_{i1}w_i + N_{i2}\left(\frac{\partial w}{\partial \bar{x}}\right)_i\right] + \sum_{i=17\sim 25}[N_{i1}w_i] = \lfloor N \rfloor \{w\}. \end{aligned} \tag{39}$$

Here, N_{ij} are the shape functions which can be determined from the specified collocation points. Also, w_i, $(\frac{\partial w}{\partial \bar{x}})_i$, $(\frac{\partial w}{\partial \bar{y}})_i$ and $(\frac{\partial^2 w}{\partial \bar{x}\partial \bar{y}})_i$ are the local degrees of freedom associated with node i.

In Kirchhoff's plate theory, the bending strain of the element is given by:

Table 3
Degrees of freedom for 25-node quadrature plate element

Nodal no.	Degrees of Freedom
1, 5, 9, 13	w, $\partial w/\partial x$, $\partial w/\partial y$, $\partial^2 w/\partial x \partial y$
2, 3, 4, 10, 11, 12	w, $\partial w/\partial y$
6, 7, 8, 14, 15, 16	w, $\partial w/\partial x$
17–25	w
Total D.o.F.	49

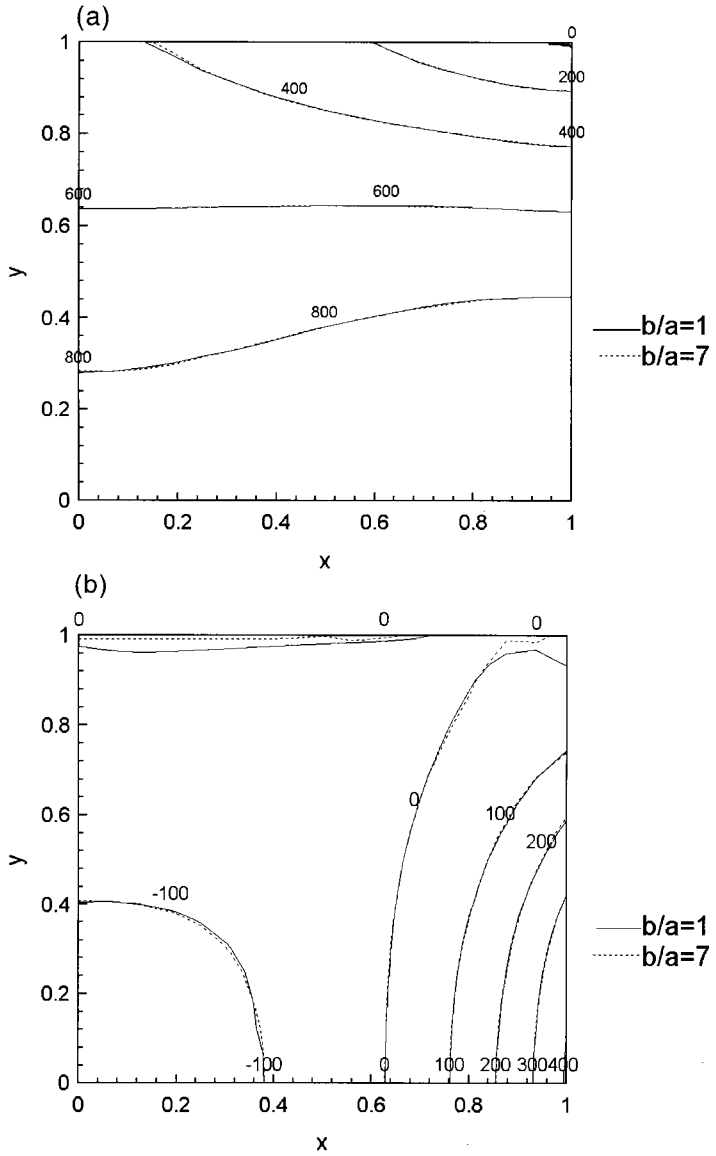

Fig. 7. (a) Isostress curves for maximum principal stress for two different grid models, (b) isostress curves for minimum principal stress for two different grid models.

$$\{\varepsilon\} = \begin{Bmatrix} \varepsilon_x \\ \varepsilon_y \\ \gamma_{xy} \end{Bmatrix} = -z \begin{Bmatrix} \dfrac{\partial^2 w}{\partial x^2} \\ \dfrac{\partial^2 w}{\partial y^2} \\ 2\dfrac{\partial^2 w}{\partial x \partial y} \end{Bmatrix}. \tag{40}$$

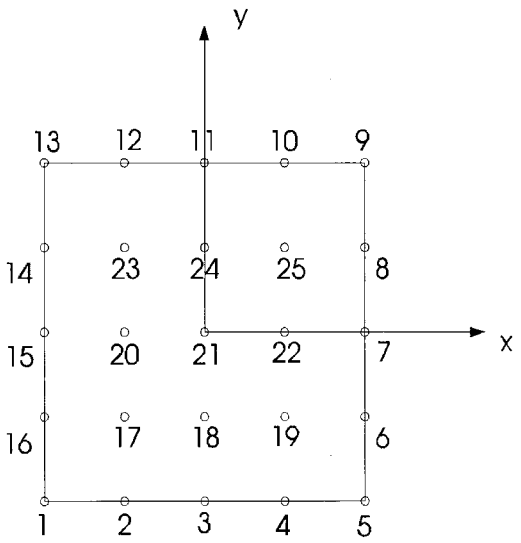

Fig. 8. Nodal configuration of quadrature plate element.

Combining Eqs. (39) and (40), one can express the strain–displacement relationship as

$$\{\varepsilon\} = -z\left\{\frac{\partial^2}{\partial x^2}\ \frac{\partial^2}{\partial y^2}\ 2\frac{\partial^2}{\partial x \partial y}\right\}^T \lfloor N \rfloor \{w\} = -z\lfloor Q \rfloor \{w\}. \tag{41}$$

For constant thickness h, the stiffness matrix can be calculated as

$$[K] = \int_A [Q]^T [D][Q] \mathrm{d}A, \tag{42}$$

in which A is the mid-surface area of the element, and $[D]$ is the rigidity matrix,

$$[D] = \frac{Eh^2}{12(1-\nu^2)} \begin{bmatrix} 1 & \nu & 0 \\ \nu & 1 & 0 \\ 0 & 0 & \dfrac{(1-\nu)}{2} \end{bmatrix}. \tag{43}$$

Because of the imposed compatibility conditions, the calculation of the stiffness matrix is more complicated and difficult to achieve analytically than that of a second-order system. When analytical calculation of the stiffness matrix becomes too complicated or even impossible, full numerical integration should be used.

The force vector can be calculated as

$$\{F\} = \int_A F(x,y) \lfloor N \rfloor^T \mathrm{d}A. \tag{44}$$

Therefore, the plate bending governing equations in matrix form can be written as

$$[K_s]\{w\} = \{F_s\}, \tag{45}$$

where the subscript s represents the whole discretized system.

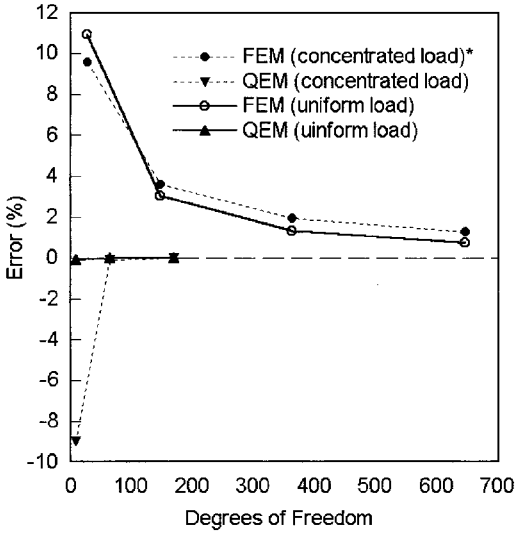

Fig. 9. Convergence comparison of QEM clamped plate model under concentrated load or uniform load. *FEM (using D.O.F. plate elements).

4.2. Numerical applications

The overall stiffness matrix and force vector in Eq. (45) are obtained by full numerical integration and assembly procedures as used in the FEM for the solution of plate bending problems. Various loading and boundary conditions are investigated in the following study. For the QEM, the domain decomposition is achieved by using Galerkin techniques; therefore, interelement C^2 and C^3 compatibility conditions are not considered here.

4.3. Results and discussion

4.3.1. Comparison with conventional low-order FEM

Consider an $a \times a$ clamped square plate under an uniform loading or a concentrated load. The coordinates used here are the same as those shown in Fig. 8. Numerical results using 49 D.o.F. QEM and 12 D.o.F. FEM plate elements are compared in Fig. 9. As expected, the QEM demonstrates superior performance in calculating the field variable for the fourth-order system. From Fig. 9, it should be noted that, when just a single element is used, the numerical results for the distributed load case are much better than those for the concentrate load case, since the element continuous basis functions are not suitable to deal with discontinuous loading conditions. However, when the discontinuity is placed on an interelement nodal point, convergence is much faster than for the low-order FEM scheme.

Table 4
Deflection of simply supported plate under central concentrated load ($w \times 100\mathrm{D}/Pa^2$, even spacing, $y = 0$)

No. of elements	D.o.F.	$(w)_{x=0}$	$(w)_{x=a/8}$	$(w)_{x=2a/8}$	$(w)_{x=3a/8}$
1×1	25	1.10961	—	0.717970	—
2×2	100	1.15812	1.00644	0.714091	0.366446
Exact		1.16004	1.00662	0.713923	0.366843

Table 5
Deflection of simply supported plate under central concentrated load ($w \times 100D/Pa^2$, Chebyshev spacing, $y = 0$, $x_n = [1-\cos(n\pi/4)]a/4$)

No. of elements	D.o.F.	$(w)_{x1}$	$(w)_{x2}$	$(w)_{x3}$	$(w)_{x4}$
2×2	100	1.15806	1.09726	0.713828	0.215204
Exact		1.16004	1.09610	0.713923	0.216007

4.3.2. Bending moment; errors at interfaces

For a more detailed test, an analytical solution for a simply supported square plate under a central concentrated load or a uniform load is calculated according to Timoshenko and Woinowsky-Krieger (1959) with up to six figures of accuracy. The coordinate system is the same as that in Fig. 8. Numerical deflection results for a simply supported plate under a central concentrated load for even and Chebyshev grid spacings are listed in Tables 4 and 5, respectively. High accuracy and good convergence are obtained similar to those for the clamped boundary condition. In addition, Table 6 shows that the QEM provides very high accuracy in calculating the bending moment which is more important in engineering applications. The deformed surface of a simply supported plate under a central concentrated load is shown in Fig. 10(a). The error distribution of the field variable, w, for a 2×2 element QEM model is shown in Fig. 10(b). The normalized error is defined as

$$\frac{(w_{\text{computational}} - w_{\text{exact}})}{w_{c\ \text{exact}}},\ w_c \equiv (0.5, 0.5). \tag{46}$$

One can observe that the largest errors occur at the interelement interfaces, since enforcement of the interpolant continuities are limited to C^0 and C^1. The compatibility conditions can be improved by increasing the order of the individual elements or by refining the mesh as in the FEM. However, the numerical results are very accurate compared to the analytical solutions from Timoshenko and Woinowsky-Krieger (1959).

4.3.3. Non-rectangular computational domains

The QEM is applied to the analysis of a uniform square plate with a square central opening as shown in Fig. 11. The external edges of the plate are simply supported, the internal edges are free, and the plate is subjected to a uniformly distributed load. One quarter of the plate is considered and three quadrature elements are used in this model. The numerical results are compared with those by Tottenham (1979) using the boundary element method (BEM) and the finite difference method (FDM) and with finite element (FEM) results as demonstrated in Table 7. The QEM demonstrates good agreement with the BEM and with fine mesh FDM and FEM models.

4.3.4. Influence of singular points

The appearance of a singularity will result in slow convergence for a conventional low-order approach. On the other hand, this type of problem can yield solutions with oscillations for high-order or series-type numerical methods because of the use of global basis functions. Thus, if only one quadrature element is used for the clamped plate model under a concentrated load as discussed in Section 4.3.1, the situation is similar to other high-order numerical methods that use global basis functions over the whole computational domain. Because of the noncontinuous loading condition, a high-order approximation does, therefore, not show much advantage over the conventional low-order FEM approach (Fig. 9). However, if a 2×2 element model is used, one can put the concentrated load at the central corner point of the four elements. That is, if the present element method is applied properly, it can isolate such

Table 6
Deflection and bending moment for uniformly loaded and simply supported square plate (even spacing, $x = 0$, $y = 0$)

No. of elements	D.o.F.	$w \times 1000D/qa^4$	$M_x \times 100/qa^2$
1×1	25	4.06218	4.78916
2×2	100	4.06235	4.78863
Exact		4.06235	4.78864

discontinuities in the computational domain or on the boundary and provide rapid convergence. Similarly, in the analysis of the uniform square plate with a square central opening, one can use a three quadrature element model to isolate the discontinuous boundary conditions as demonstrated in Table 7.

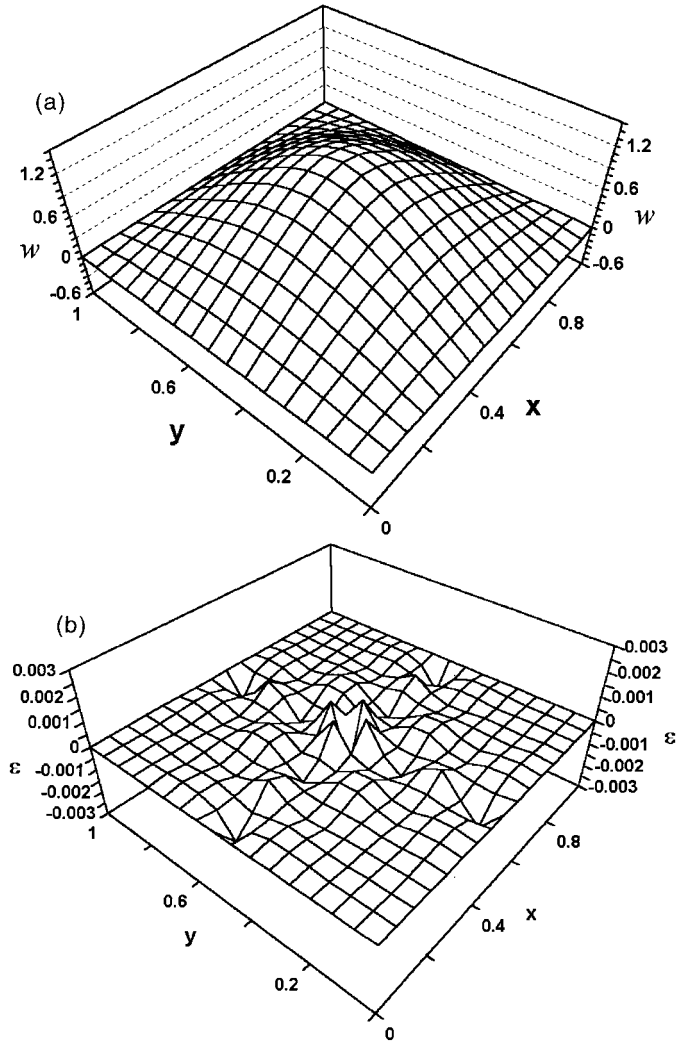

Fig. 10. (a) Numerical results for a square plate under point load — deformed surface, (b) numerical results for a square plate under point load — normalized error distribution.

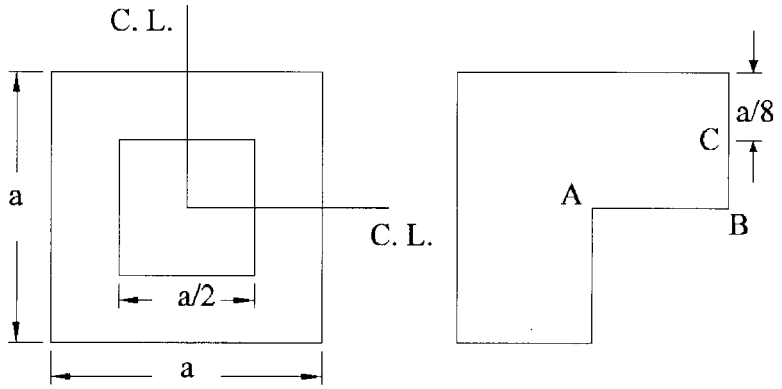

Fig. 11. Square plate with central square opening.

Table 7
Displacements for square plate with square central opening under uniform loading ($w \times 100D/qa^4$, $\nu = 0.25$)

Location	BEM [11]	FDM [11]	FEM[a] (12)[b]	FEM[a] (48)	FEM[a] (192)	QEM (3)
A	0.2188	0.2174	0.2180	0.2183	0.2187	0.2189
B	0.3107	0.3006	0.3048	0.3030	0.3025	0.3037
C	0.1558	0.1541	0.1545	0.1548	0.1548	0.1552

[a] By MSC/NASTRAN QUAD4 plate element.
[b] Number of elements.

5. Conclusions

The superior accuracy of quadrature elements as applied to second- and fourth-order elliptic problems with smooth solutions in static analysis has been demonstrated through the numerical investigations in this study. Using the techniques proposed here can result in a substantially lower computational effort for given accuracy, or, alternatively, allows one to obtain solutions with smaller errors than the standard finite element method. It is expected that the QEM as a combination of DQM and FEM will allow for a wider range of reliable applications than is commonly believed possible with other higher-oder or series-type numerical schemes.

References

Bellman, R.E., Casti, J., 1971. Differential quadrature and long-term integration. J. Math. Anal. Applic. 34, 235–238.
Bernardi, C., Maday, Y., 1991. Some spectral approximations of one-dimensional fourth orders problems. In: Neval, P., Pinkus, A. (Eds.), Problems in Approximation Theory. Academic Press, San Diego, pp. 43–116.
Bert, C.W., Jang, S.K., Striz, A.G., 1989. Nonlinear bending analysis of orthotropic rectangular plates by the method of differential quadrature. Comput. Mech. 5, 217–226.
Canuto, C., Hussaini, M.Y., Quarteroni, A., Zang, T.A., 1987. Spectral Methods in Fluid Dynamics. Springer, New York.
Chen, W.L., Striz, A.G., Bert, C.W., 1997. A new approach to the differential quadrature method for fourth-order equations. Intl. J. Numer. Meth. Engng. 40, 1941–1956.
Cowper, G.R., Lindberg, G.M., Olson, M.D., 1970. A shallow shell finite element of triangular shape. Int. J. Solids Structures 6, 1133–1156.

Jang, S.K., Bert, C.W., Striz, A.G., 1989. Application of differential quadrature to deflection and buckling of structural components. Int. J. Numer. Meth. Engng. 28, 561–577.

Patera, A., 1984. A spectral element method for fluid dynamics: laminar flow in a channel expansion. J. Comput. Phys. 54, 468–488.

Quan, J.R., Chang, C.T., 1989. New insights in solving distributed system equations by the quadrature method — I Analysis. Computers Chem. Engng. 13 (7), 779–788.

Striz, A.G., Chen, W.L., Bert, C.W., 1997. Free vibration of plates by the high-accuracy quadrature element method. J. Sound Vib. 202 (5), 689–702.

Striz, A.G., Jang, S.K., Bert, C.W., 1988. Nonlinear bending analysis of thin circular plates by differential quadrature. Thin-Walled Struct. 6, 51–62.

Timoshenko, S., Woinowsky-Krieger, W., 1959. Theory of Plates and Shells, 2nd ed., McGraw–Hill Book Company, Inc, New York.

Tottenham, H., 1979. The boundary element method for plates and shells. In: Banerjee, P.K., Butterfield, R. (Eds.), Developments in Boundary Elements, vol. I. Applied Science Publishers Ltd, London, UK, pp. 173–199.

Wang, X., Bert, C.W., Striz, A.G., 1993. Differential quadrature analysis of deflection, buckling, and free vibration of beams and rectangular plates. Comput. Struct. 48 (3), 473–479.